

Signatures of the single particle mobility edge in the ground state properties of Tonks-Girardeau and non-interacting Fermi gases in a bichromatic potential

J. Settimo,^{1,2} N. Lo Gullo,^{3,4} A. Sindona,^{1,2} J. Goold,⁵ and F. Plastina^{1,2}

¹*Dipartimento di Fisica, Università degli Studi della Calabria, Arcavacata di Rende, Italy*

²*INFN, gruppo collegato di Cosenza*

³*Dipartimento di Fisica, Università degli Studi di Milano, Milano, Italy*

⁴*INFN, sezione di Milano*

⁵*ICTP, Trieste, Italy*

We explore the ground state properties of cold atomic gases, loaded into a bichromatic lattice, focusing on the cases of non-interacting fermions and hard-core (Tonks-Girardeau) bosons, trapped by the combination of two potentials with incommensurate periods. For such systems, two limiting cases have been thoroughly established. In the tight-binding limit, the single-particle states in the lowest occupied band show a localization transition, as the strength of the second potential is increased above a certain threshold. In the continuous limit, when the tight-binding approximation does not hold anymore, a mobility edge is found, whose position in energy depends upon the strength of the second potential. Here, we study how the crossover from the discrete to the continuum behavior occurs, and prove that signatures of the localization transition and mobility edge clearly appear in the generic many-body properties of the systems. Specifically, we evaluate the momentum distribution, which is a routinely measured quantity in experiments with cold atoms, and demonstrate that, even in the presence of strong boson-boson interactions, the single particle mobility edge can be observed in the ground state properties.

I. INTRODUCTION

Ultra-cold quantum gases, now prepared in a variety of configurations in laboratories worldwide, have emerged as ideal candidates for clean and controllable simulation of condensed matter physics [1]. In particular, both Bosonic and Fermionic atoms can be loaded and manipulated on optical lattice potentials [2]. The lack of thermal phonons, coupled with the tunability of the interactions by means of Feshbach resonances [3], has allowed for the detailed study of a multitude of phase diagrams of critical many-body systems, both at equilibrium, and away from it [4, 5].

Besides the ability to engineer and tune interactions, a particularly appealing feature of cold atoms, for the simulation of condensed matter physics, is the possibility to manipulate the external potential shapes. In this respect, this paper will focus on many-body systems in a *quasi-periodic geometry*, implemented via an external potential that realizes what is known as André-Aubry (AA) model [6–9, 12–16]. This is a one dimensional tight binding model on a lattice, with nearest-neighbor hopping terms and on-site energies given by a combination of two periodic functions having non-commensurate wave numbers, which has been shown to display a metal-to-insulator transition [7, 8].

The interplay between geometry and interaction in many-body systems can generate an impressive range of physical phenomena. For example, the ground state properties of interacting bosons, subject to a quasi-periodic potential, show a rich phase diagram at zero temperature [17–19], displaying superfluid, Bose-glass and Mott insulator phases depending upon the filling of the lattice, the interactions and the strength of the potential. Interestingly, a mobility edge (ME) appears when an extension of the AA model is considered, allowing for longer-range hopping such as next-nearest-neighbor terms [20–22] or a continuous model (infinite-range hopping)[23, 24], or even interactions [25]. The extended-to-

localized phase transition of the AA model, within the framework of many body physics, has been widely investigated both from a theoretical point of view [26–29] and also from an experimental perspective [33–39].

In this work, we ask how the presence of a ME in the single particle problem affects many-body measurable quantities, and to what extent the latter can be used to detect it. To this aim, we study the ground state properties of both non-interacting fermions and of strongly-interacting bosons in a bichromatic lattice. After having briefly described the fermion-based representation of the strongly interacting boson gas in Sec. II, thus motivating the choice of looking at both of the species, in Sec. III we introduce the model considered and recall the single particle properties, which are crucial to understand the results in the many-body case. Then, in Sec. IV and Sec. V, we describe the effect of the delocalization-to-localization transition, and of the mobility edge on the many-body ground state, for a system of non-interacting spinless fermions and for a Tonks-Girardeau gas.

II. THE TONKS-GIRARDEAU GAS

Optical lattices allow to create trapping potentials that are tight enough in the transversal direction to freeze out all dynamics in these degrees of freedom [30]. A gas of N bosons in such a potential can then be approximated by the one-dimensional Hamiltonian

$$\mathcal{H}_0 = \sum_{n=1}^N \left[-\frac{\hbar^2}{2m} \frac{\partial^2}{\partial x_n^2} + V_{ext}(x_n) \right] + g_{1D} \sum_{i<j} \delta(|x_i - x_j|)$$

where m is the mass of the particles, V_{ext} is the trapping potential and g_{1D} is a 1D coupling constant which is derived from the renormalisation of the three-dimensional scattering process, $g_{1D} = \frac{4\hbar^2 a_{3D}}{ma_{\perp}} (a_{\perp} - Ca_{3D})^{-1}$ [31]. Here a_{\perp} is the trap width and $C = -\zeta(1/2) \simeq 1.46035$ is a constant.

This Hamiltonian describes an inhomogeneous Lieb-Liniger gas, which in the strongly repulsive limit, $g_{1D} \rightarrow \infty$, can be solved by using a mapping to an ideal and spinless fermionic system [32]. The essential idea of this mapping is that one can then treat the interaction term in Eq. (1) by replacing it with a boundary condition on the allowed Bosonic wave-function

$$\Psi_B(x_1, x_2, \dots, x_n) = 0 \quad \text{if} \quad |x_i - x_j| = 0, \quad (2)$$

for $i \neq j$ and $1 \leq i \leq j \leq N$. This is the hard core constraint, which says that no probability exists for two particles ever to be at the same point in space.

Such a constraint is automatically fulfilled by calculating the wave-function using a Slater determinant

$$\Psi_F(x_1, x_2, \dots, x_N) = \frac{1}{\sqrt{N!}} \det_{(n,j)=(0,1)}^{(N-1,N)} \psi_n(x_j), \quad (3)$$

where the ψ_n are the single particle eigenstates of the ideal system. This, however, leads to a fermionic rather than bosonic symmetry, which can be corrected by a multiplication with the appropriate unit antisymmetric function [32]

$$A = \prod_{1 \leq i < j \leq N} \text{sgn}(x_i - x_j), \quad (4)$$

to give $\Psi_B = A\Psi_F$. Once the single particle eigenstates of the system in the external potential of interest are known then the many-body properties of both the free Fermionic and hard-core Bosonic systems can be investigated.

III. SINGLE PARTICLE PROBLEM

Let us consider the time independent Schrödinger equation for a particle in an external potential:

$$\left[-\frac{\hbar^2}{2m} \frac{\partial^2}{\partial x^2} + V_{ext}(x) \right] \psi_n(x) = e_n \psi_n(x). \quad (5)$$

In what follows, we will consider an external potential which describes a bichromatic lattice,

$$V_{ext} = V_1 \sin^2(k_1 x) + V_2 \sin^2(k_2 x). \quad (6)$$

Although any irrational number would work as well, to be specific we will take $\frac{k_1}{k_2} = \frac{1+\sqrt{5}}{2} = \tau$, the golden ratio, and assume $V_1 > V_2$. For $V_2 = 0$ and $V_1 \geq 5E_{R_1}$ it is possible to resort to the so called tight-binding (TB) limit to approximately describe the system. Here $E_{R_1} = \hbar^2 k_1^2 / (2m)$ is the recoil energy, giving an estimation of the energy at which the potential with modulation V_1 opens the first gap of width $\propto V_1$ in the otherwise gapless free particle spectrum (for $V_1 = V_2 = 0$). The above condition therefore ensures that all particles with energy $E < E_{R_1}$ do not have enough energy to overcome the first gap and, therefore, that they are confined in the lowest band of the potential. In this limit, the properties of the system are dominated by the external potential and it is possible to rewrite the single particle Hamiltonian in Eq. (5) in terms of

states $|i\rangle$, localized around the minima of the potential, whose wave functions $w_i(x) = \langle x|i\rangle$ are the so called Wannier functions. In the presence of the second potential $V_2 < V_1$, and in the TB limit, the continuum model described by Eq. (5) can be mapped into the so called Aubry-Andre (AA) model:

$$\hat{H} = \Delta \sum_j \cos(2\pi\tau j) |j\rangle\langle j| - J \sum_j (|j+1\rangle\langle j| + |j\rangle\langle j+1|). \quad (7)$$

The first term on the r.h.s., proportional to Δ , accounts for the on-site energy, whereas the second one, proportional to the hopping constant J , is responsible for nearest-neighbor tunnelling between adjacent sites. Both Δ and J depend upon the choice of the set of Wannier functions, which in turn depend upon the first potential only if the condition $V_2 \ll V_1$ is satisfied.

The AA model has been widely studied from different points of view. For what we are concerned here, it is worth recalling that the AA model shows a delocalized-to-localized (or metal-to-insulator) transition at $\Delta/J = 2$. This point marks the change from a delocalized phase ($\Delta/J < 2$), in which all of the eigenstates have an extended character with a corresponding absolutely continuous spectrum, to a phase where all states are localized and the spectrum is discrete [9]. As for the many-body properties of this system, it has been predicted numerically and verified experimentally that bosons with the addition of on-site interaction in the AA model enjoy a particularly rich phase diagram, which includes a superfluid to Bose-glass transition at low filling, and also a Mott insulator phase for higher filling and interaction strength.

In the continuum, outside the range of validity of the TB approximation, it is known that the sharp delocalized-to-localized transition of the lowest energy band transforms into a mobility edge, whose position in energy changes with V_2 [20, 21]. Our aim is to study in detail how this crossover from the discrete to the continuum behavior occurs, and to show that signatures of this transition are displayed in the many-body properties of both non-interacting fermions and strongly-interacting bosons. We will therefore always work with the continuous model of Eq. (5) and move from the discrete to the continuous limits by changing the strength of the main potential V_1 . For each set of parameters $\{V_1, V_2\}$ we have numerically solved the eigenvalue problem given by Eq. (5) via a fifth order Matrix Numerov Method [40], considering systems with $N = 100$ lattice sites and total length $k_1 L = 100\pi$.

A. Mobility edge in the single particle problem

In the discrete model, all of the eigenfunctions of the Hamiltonian of Eq. (5) in the TB regime are either extended or localized, depending on whether the value of V_2 is below or above a certain characteristic value V_2^t . On the other hand, if $V_1 < 5E_R$ a Mobility Edge (ME) appears such that, for a fixed value of V_2 , states with energy lower than the ME are localized whilst the others are delocalized [23]. The ME is found at higher energies for increasing V_2 . It is possible to

obtain an estimation of the localization threshold V_2^t by calculating explicitly Δ and J of the AA model – as a function of V_1 and V_2 – and inverting the condition $\Delta/J = 2$, by solving for V_2 . Using the numerical estimations given in [6], we have obtained

$$V_2^t = 2E_{R_2} 14.9752e^{\frac{0.381966}{\sqrt{V_1/E_{R_1}}} - 2.07\sqrt{V_1/E_{R_1}}} (V_1/E_{R_1})^{0.98} \quad (8)$$

In the following we will use the rescaled quantity $v_2 = V_2/V_2^t$ in order to compare systems with different V_1 and V_2 . This guarantees that the transition point in the TB limit always occurs at $v_2 = 1$. However, it is important to notice that the computation of V_2^t has been done, and it is meaningful only in the TB limit. As we will also consider parameters for which the TB approximation does not hold, then the value $v_2 = 1$ will lose its importance and its role of transition point. To quantitatively discuss the transition in the general case, we will employ the Inverse Participation Ratio $\text{IPR}(\psi) = \int |\psi(x)|^4 dx / \int |\psi(x)|^2 dx$ for the eigenfunctions of the first energy band of the Hamiltonian. This quantity measures the inverse of the average spatial region occupied by the eigenfunction. We will consider an eigenfunction to be localized if its IPR is larger than $1/(5l)$ where l is the distance between two neighbor lattice sites. Fig. 1 shows the number of localized states as a function of V_2 for different values of V_1 : in the TB regime (upper, red curve) the transition is sharp, whereas in the continuum there is an ME, as witnessed by the plateaux in Fig. 1, that correspond to gaps inside the first energy band. Moreover, as anticipated above, Fig. 1 shows that the estimation of the transition point V_2^t given in Eq. (8) fails when the TB description does not provide a good approximation (see, e.g. the lower curve, corresponding to $V_1 = E_R$). We finally show in Fig. 2 the IPR of the ground state wave function, normalized to one lattice length, together with the function itself and its Fourier transform for various values of v_2 .

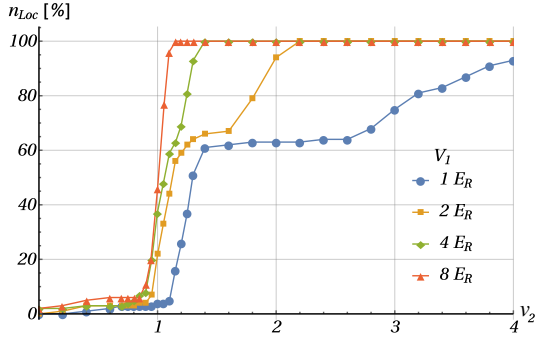


Figure 1. (Color online) Number of localized states as a function of v_2 for different values of V_1 . An eigenfunction is considered to be localized if its IPR is greater than $1/5l$ where l is the distance between two neighboring sites. For the system considered here, $5l$ corresponds to the 5% of the whole lattice length L .

In the remainder of the paper we will show how both the sharp transition, occurring in the TB limit, and the appearance of the ME affect the many-body properties of non-interacting

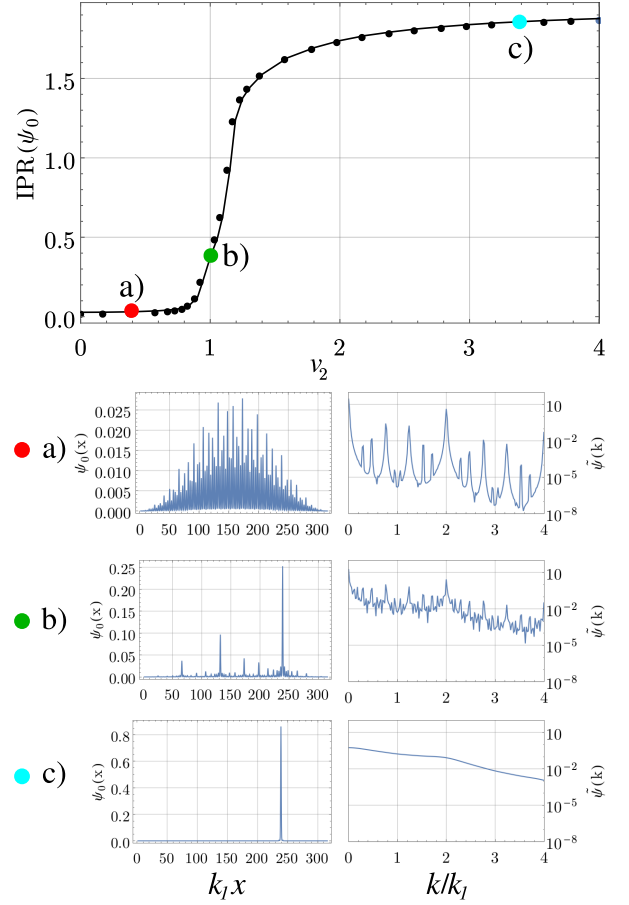


Figure 2. (Color online). (Top) Normalized IPR of the single particle ground state of the system as a function of v_2 for $V_1 = 8E_R$. (Bottom) Single particle ground state and its Fourier Transform in the delocalized, critical and localized regions corresponding to the values of v_2 reported in red, green and cyan colors, respectively, in the top figure.

spinless fermions and Tonks-Girardeau bosons. It is known that the excitation spectrum of the Tonks-Girardeau model is the same as that of non-interacting spinless fermions and that all local quantities are the same for the two systems. On the other hand, non local quantities, such as the momentum distribution, are different and reveal the fermionic and bosonic nature of the two systems. More importantly, we shall see that the different statistical nature of the two kind of particles also shows up in the way the localization transition and the appearance of the ME manifest themselves in the momentum distributions.

IV. FERMIONS IN A BICHROMATIC LATTICE

In this section, we consider the effect of the ME of the single-particle spectrum on the ground state properties of a system of N non-interacting fermions loaded into the bichromatic lattice, and, more generally, discuss the signatures of the transition from discrete to continuum, occurring as V_1 is

decreased.

The many-body wavefunction describing a system of N non-interacting spinless fermions is given by a Slater determinant of single particle states (see Eq. (3)). Below, we focus on the reduced single particle density matrix (RSPDM)

$$\rho_F(x, y) = \int dx_2 \dots dx_N \Psi_F^*(x, \dots, x_N) \Psi_F(y, \dots, x_N), \quad (9)$$

whose knowledge is sufficient to evaluate the expectation values of all single-particle operators. Its Fourier transform gives the momentum distribution (MD),

$$n_F(k) = \frac{1}{2\pi} \int dx dy \exp^{ik(x-y)} \rho_F(x, y), \quad (10)$$

which is directly measurable in cold atom experiments. The eigenfunctions ($\phi_i(x)$) and eigenvalues (λ_i) of the RSPDM, defined by $\int dx \rho_F(x, y) \phi_i(x) = \lambda_i \phi_i(y)$, and normalized such that $\sum_i \lambda_i = 1$, are the so called *natural orbitals* and their populations, respectively. For a non-interacting Fermi gas, as one could have expected, there are only N non-vanishing eigenvalues, which are all equal to one, and the corresponding eigenvectors coincide with the first N lowest single particle energy states. A similar analysis for a Tonk-Girardeau gas will prove to be much less trivial.

The RSPDM and MD of a non-interacting fermion gas in its ground many-body state can be expressed via the single particle energy eigenstates: $\rho_F(x, y) = \sum_{j=1}^N \psi_j^*(x) \psi_j(y)$ and $n(k) = \sum_{j=1}^N |\tilde{\psi}_j(k)|^2$ where $\tilde{\psi}_j(k)$ is the Fourier transform of $\psi_j(x)$ [41].

We analyze the TB limit first, where, interestingly enough, the MD offers a signature of the localization transition inherited from the single particle properties. On the delocalized side, the Fourier transform of each single particle state displays peaks at the wave numbers $k(m, n) = 2mk_1 \pm 2nk_2$ with $m, n \in \mathbb{Z}$, and the MD shows several Fermi-Dirac-like flat structures due to the occupation of states with nearby momentum peaks. This is shown in Fig. 3, where explicit reference to gases of $N = 15$ and $N = 65$ fermions is made. In the delocalized region ($v_2 < 1$), indeed, some nearly flat regions appear in the MD. They are centered at different $k(n, m)$'s, and are due to the fact that each single particle wavefunction contributes with at least two momenta (but in general more, for higher energy states); these momenta pile up in the total $n(k)$ to give a sequence of nearby peaks forming these Fermi-Dirac-like (almost) flat regions, whose width is proportional to the number of particles.

On the other hand, again in the TB regime, but now in the localized domain, the MD suddenly smoothens for $v_2 > 1$, due to the fact that single particle states are all localized, so that their Fourier transform flattens over in momentum space. Before shifting our attention to the continuum case, it is instructive to discuss the nature and origin of the structures that appear at the edges of the flat regions. They are particularly well visible in the case of $N = 65$. Conversely, for $N = 15$, they only show up as small peaks, whose height increases with increasing v_2 until the transition point $v_2 = 1$ is reached, where they disappear leaving structure-less bumps.

To understand why this happens, we recall that the addition of the second potential leads to a fragmentation of the energy spectrum into sub-bands separated by gaps whose width depends, at first order in a perturbation analysis, on the amplitudes of the Fourier transform of the potential itself. Furthermore, the sub-bands tend to flatten out as the potential is increased. This implies that the density of states increases at the sub-band edges and more particles can be accommodated there. As a result, the structures at the edges of the flat regions become better and better defined as the number of particles increases.

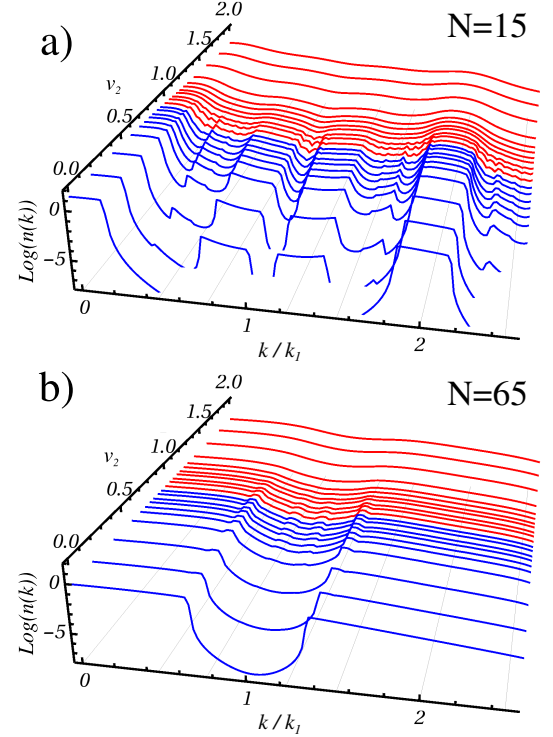


Figure 3. (Color online). Momentum distribution $n(k)$ as a function of v_2 for a system of non-interacting fermions with $V_1 = 8E_r$ (TB limit). The two panels refer to a different number of fermions: a) $N=15$ and b) $N=65$. Blue and red curves are for $v_2 < 1$ and $v_2 > 1$ respectively.

In the continuum, namely $V_1 \approx E_R$, the delocalized-to-localized transition turns into the appearance of an ME. Indeed, Fig. 4 b) shows that it is possible to observe structures in the MD of an $N = 65$ fermion gas at any value of v_2 , and in particular well beyond the transition point $v_2 = 1$, which used to mark a sharp transition in the TB approximation. The persistence of such structures is a signature of the existence of occupied single particle states, which remain delocalized beyond $v_2 = 1$.

However, this seems not to be the case if one looks at Fig. 4 a), where $n(k)$ is shown for $N = 15$ fermions, instead. Here, the structures of the MD quickly disappear when increasing v_2 beyond 1. In fact, as we considered a smaller number of fermions in this case, less states are occupied, and all of them become localized for $v_2 > 1$ (giving rise to a quick smooth-

ing of $n(k)$). The comparison between Fig. 4 a) and Fig. 4 b), therefore, shows that, in the same band, there exist both localized single particle states (at low energy) and delocalized ones (at higher energy), which is a clear manifestation of the ME.

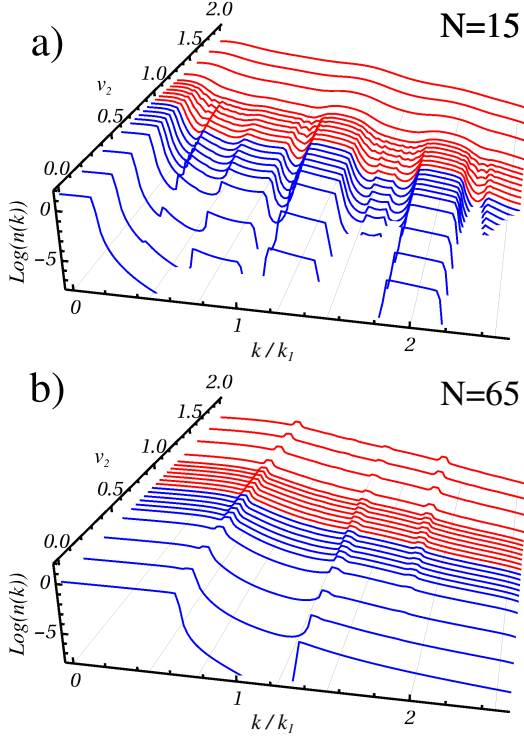


Figure 4. (Color online). $n(k)$ as a function of v_2 for a system of non-interacting fermions with $V_1 = 8E_r$. The same parameters and coloring as Fig. 3 is used. A persistence of the edge-structures well beyond $v_2 = 1$ is observed for $N = 65$, but not for $N = 15$ as, for these parameters, the first 15 single particle states remain below the ME.

In order to characterize quantitatively this phenomenon, we resort to an approach already used in Ref.[10] to study the degree of delocalization of phonon modes in quasi-crystalline structures. The idea behind it is to evaluate the area under the MD peaks, in order to quantify the total power spectrum coming from coherent sources, which in our case correspond to delocalized single particle states. Therefore, we have evaluated the total area I_d below the edge-peaks in $n(k)$ after removing the background. On the delocalized side ($v_2 < 1$) I_d increases as a function of v_2 due to the appearance of new peaks, induced in the single particle states by the second potential, when the transition point is approached. Moreover, for small numbers of fermions ($N = 15$) such an increase is approximately linear, up until saturation is reached. This behavior stems from the fact that only the lower energy eigenstates are occupied and, therefore, large values of the second potential are needed to make them develop a spatial structure, which involves more momenta. On the other hand, for $N = 65$, saturation occurs well before, due to the fact that higher energy eigenstates are occupied even at small values of v_2 , which contribute to $n(k)$ with more momenta and, therefore, more

peaks.

When the localized eigenstates start to be occupied, I_d decreases due to the smoothing of the MD profile. In the TB-regime, I_d suddenly goes to zero for $v_2 > 1$, regardless of the number of fermions, as all of the eigenstates suddenly localize. On the other hand, in the continuous limit with $V_1 \approx E_r$, we observe the appearance of an ME as I_d decreases for $v_2 > 1$ and reaches a plateau (blue and yellow curves in Fig. 5 b). The plateaux, in particular, witness the ME moving through the band towards higher energies.

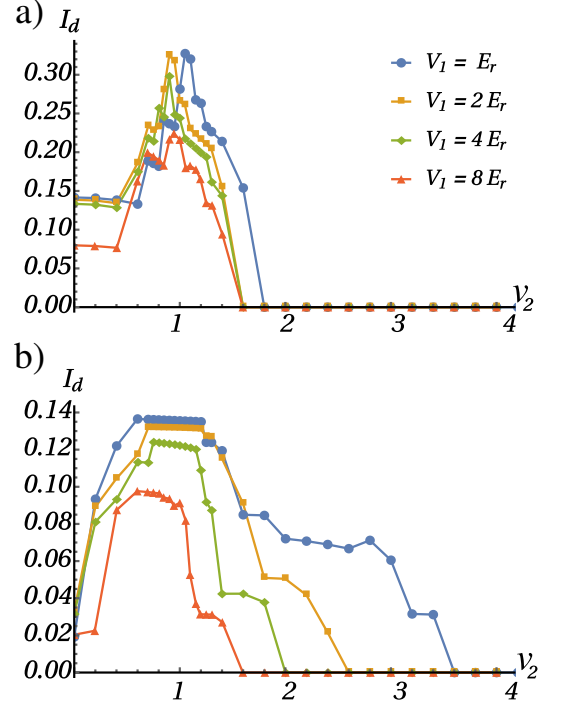


Figure 5. (Color online). I_d for a) $N_p = 15$ and b) $N_p = 65$ fermions.

V. TONKS-GIRARDEAU GAS IN A BICHROMATIC LATTICE

In Sec.IV we have seen that signatures of the ME appear in the momentum distribution of the the RSPDM of a many-body system of spinless fermions. In this section we look at a strongly-interacting boson gas (i.e., the Tonks-Girardeau gas), whose ground state properties can be related to the fermionic ones via the prescription outlined in Sec.II.

The many body spectrum of a hard-core boson system is, in fact, the same as that of the noninteracting fermion gas, loaded into the same optical potential $V(x)$. Moreover, it is possible to show that the mapping from hard-core bosons to non-interacting fermions leaves all *local* quantities unchanged; for instance, given the many-body wavefunction for N hard-core bosons, the density of bosons is the same as that of N non interacting fermions. Conversely, non-local properties, such as correlation functions, are different in the

two cases. For this reason we expect the MD, which is derived from the off-diagonal entries of the RSPDM, to be markedly different from that observed in Sec.IV, because of the presence of spatial coherences, typical of a boson gas.

In Ref. [41], it has been shown that the RSPDM of N hard-core bosons can be obtained by the single particle eigenstates of the equivalent non-interacting fermion problem as:

$$\rho_B(x, y) = \sum_{i,j=1}^N \psi_i^*(x) A_{ij}(x, y) \psi_j(y) \quad (11)$$

where $A_{ij}(x, y) = (\mathbf{P}(x, y)^{-1})_{ji} \det(\mathbf{P}(x, y))$ and the $N \times N$ matrix \mathbf{P} is given by $P_{ij}(x, y) = \delta_{ij} - 2 \int_x^y dx' \psi_i^*(x') \psi_j(x')$. As in the fermionic case, the many-body MD is obtained by a Fourier transform of the RSPDM, $n_B(k) = \frac{1}{2\pi} \int dx dy \exp^{ik(x-y)} \rho_B(x, y)$.

The MD is conveniently expressed in terms of the natural orbitals and their corresponding eigenvalues, $n(k) = \sum_{j=1}^N \lambda_j |\tilde{\phi}_j(k)|^2$. Here, $\tilde{\phi}_j(k)$ is the Fourier transform of the j -th natural orbital, given by the eigenfunction of the RSPDM: $\int dx \rho_B(x, y) \phi_j(x) = \lambda_j \phi_j(y)$.

As expected, the bosonic MD is markedly different from that of the non-interacting fermion case. Due to their bosonic nature, at zero temperature the particles would tend to occupy the single particle modes with lowest energy. On the other hand, due to the very strong repulsion between two bosons when their spatial overlap is large, particles tend to occupy states in order to lower their overlap. The interplay between these two effects is the key mechanism that explains the behavior of the MD for strongly interacting bosons, which we will now analyze.

On the delocalized side $v_2 < 1$, the sharp peaks of the non-interacting fermion case are replaced by broad peaks centered at specific momenta of the form $k(m, n) = 2mk_1 + 2nk_2$, induced by the trapping potential.

Indeed, as stated above, bosons would want to occupy a low energy mode, but not all can occupy the same one, as this would lead to a large overlap between their wavefunctions and, therefore, to an increase of the total energy. This effect is taken into account by the presence of the factors A_{ij} in the RSPD matrix, as built from single particle eigenfunctions in Eq.11. Such a behavior gets more and more pronounced with increasing the number of bosons, as witnessed by panel a) and b) in Fig. 6, where we display the MD for $V_1 = 8E_r$ in a system of $N = 15$ and $N = 65$ bosons as a function of v_2 . In the first case [Fig. 6 a), $N = 15$], two new peaks appear as the second potential is switched on, which are very well pronounced and persist up until the transition point $v_2 = 1$ is reached. For $v_2 > 1$, instead, the peaks broaden, $n(k)$ smoothen out and any structure is lost.

In the second case [Fig. 6 b), $N = 65$], the two peaks emerge from an already large background, which is due to the large number of bosons in the system that tend to occupy more states. This implies that the tails of the main peaks, due to the main potential V_1 , are quite high. Notwithstanding the fact that they are immersed in these tails, they are still visible, therefore witnessing the spatial coherence of delocalized modes.

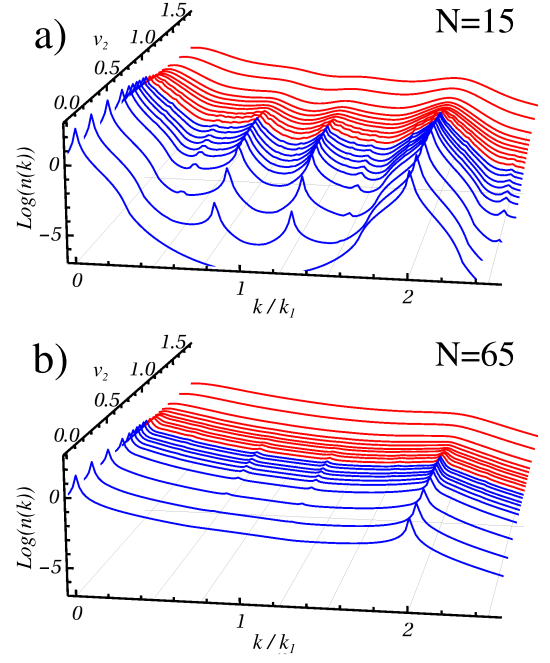


Figure 6. (Color online). Momentum distribution $n(k)$ as a function of v_2 for a system of strongly-interacting bosons with $V_1 = 8E_r$ (TB limit). Different figures refer to a different number of bosons: a) $N=15$ and b) $N=65$. Blue and red curves are for $v_2 < 1$ and $v_2 > 1$ respectively.

To better highlight such structures, we performed a peak-area analysis, similar to that discussed for fermions. Fig. 8b shows that for $V_1 < 4E_r$ the areas under the discrete part of the MD does not go to zero at the transition point, confirming the presence of the ME.

Unlike the non-interacting fermion case, where the occupancy of each natural orbital was either 0 or 1, here it is meaningful to look at their distribution and at the entropy of the RSPDM given by $S(\rho_B) = -\sum_i \lambda_i \ln \lambda_i$. For N strongly interacting bosons at the absolute zero, we should not always expect that the first N energy levels are occupied, and, correspondingly, $S(\rho_B) \neq \ln N$. However, we expect the entropy to reach such a value in the *localized phase*, where *i*) the eigenstates are exponentially localized in space and, therefore, the strong interaction forbids more than one boson to occupy an energy level, and *ii*) there is a one-to-one correspondence between energy eigenfunctions and natural orbitals. As a result, the occupancy of the first N natural orbitals is 1, as for fermions, and the entropy is $\ln N$. On the other hand, in the delocalised phase, the occupation of natural orbitals changes, with λ_i decreasing almost-exponentially with i , and the entropy can take on an arbitrary value $S(\rho_B) > 0$. For weakly interacting bosons at zero temperature, in the superfluid phase, we have $S(\rho_B) \ll \ln N$ because they all tend to occupy the same energy level. As the interaction is increased (but always remaining within the superfluid phase), we expect bosons to spread in the Hilbert space, resulting in the occupancy of other natural orbitals, allowing for a more dilute distribution. This, in turn, leads to $S(\rho_B) > \ln N$. In Fig. 9 we show the entropy

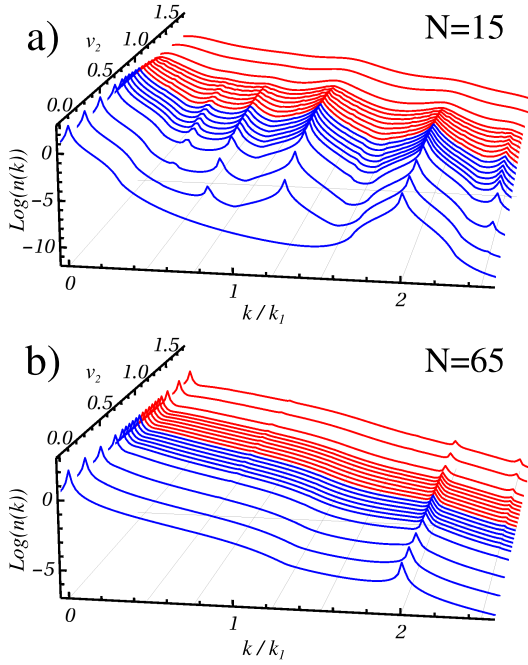


Figure 7. (Color online). Momentum distribution $n(k)$ as a function of v_2 for a system of strongly-interacting bosons with $V_1 = E_r$. Different figures refer to a different number of bosons: a) $N=15$ and b) $N=65$. Blue and red curves are for $v_2 < 1$ and $v_2 > 1$ respectively.

$S(\rho_B)/\ln N$ as a function of v_2 and for different values of the main potential strength V_1 going from the TB to the continuum limits, for the cases of $N = 15$ [Fig. 9 a)], and $N = 65$ bosons [Fig. 9 b)]. It can be seen that, as expected, deep in the localized phase $v_2 > 1$, the entropy tends to $\ln N$, showing that bosons tend to occupy one natural orbital each. It is interesting to compare the behavior of the entropy for $v_2 < 1$ for low and large numbers of Bosons. In the first case (e.g., $N = 15$), the entropy is smaller than $\ln 1$ away from the transition point $v_2 \approx 1$, while it exceeds this value around it. In the second case (e.g. $N = 65$), the entropy exceeds $\ln N$ even in the delocalized phase for $V_1 \gg E_r$ (TB limit). In this limit, indeed, the eigenfunctions are delocalized across the whole system, but their amplitudes show an increase around the minima of the main potential (i.e. V_1). Therefore two bosons residing in the same single particle eigenfunction would both be localized around the minima; as the interaction increases they naturally tend to occupy other excited states in order to reduce the average overlap of their wavefunctions. This is why they would tend to occupy more eigenstates, resulting in a number of occupied natural orbitals larger than N . On the other hand, as the system is brought in the continuous limit (e.g., for $V_1 \approx E_r$), bosons are allowed to also occupy regions between the minima of the potential, and therefore the above effect is less important and the entropy drops below $\ln N$.

Furthermore we can see that the entropy signals the presence of the ME. To see this we again compare the two cases $N = 15$ and $N = 65$ for $V_1 = E_r$ (blue circles in Fig. 9). In the first case, the entropy rapidly reaches the asymptotic value $\ln N$, showing the fermion-like behavior of bosons which oc-

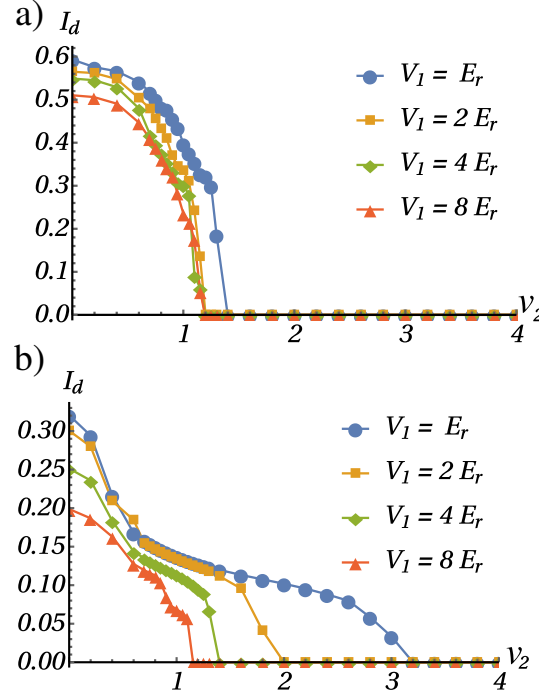


Figure 8. (Color online). Area under the discrete peaks, I_d , as a function of v_2 for various values of V_1 , and for a) $N_p = 15$ and b) $N_p = 65$ bosons.

cupy one natural orbital each. Conversely, for $N_p = 65$ the asymptotic value is attained for higher values of v_2 , showing that some delocalized states are occupied.

We can also consider the behavior of the largest eigenvalue λ_k of the RSPDM (Fig. 10). As expected, in the localized phase it asymptotically goes to 1 (as all the first N eigenvalues do), whereas in the delocalized region it becomes larger than one. Once again the presence of the ME in the continuum is witnessed by the fact that λ_k does not decay suddenly as a function of v_2 (blue circles in Fig. 8 b)).

VI. CONCLUSIONS

We have studied the many-body ground state properties of a system of non-interacting fermions and strongly interacting bosons in a one-dimensional bichromatic potential. In the tight-binding regime we have seen that signatures of the transition are clearly manifested in the many-body properties of both systems. Similarly, the presence of a mobility edge in the continuum changes the many-body properties of the ground state, as shown by comparing the momentum distribution for different numbers of particles in the system. If the number of particles is such that only levels below the mobility edge are filled, then the behavior of the system is similar to that in the tight-binding regime, as all occupied states suddenly localize. On the other hand, an increase in the number of particles results in the mobility edge crossing the region of the occupied states as the second potential is varied. This is clearly visible

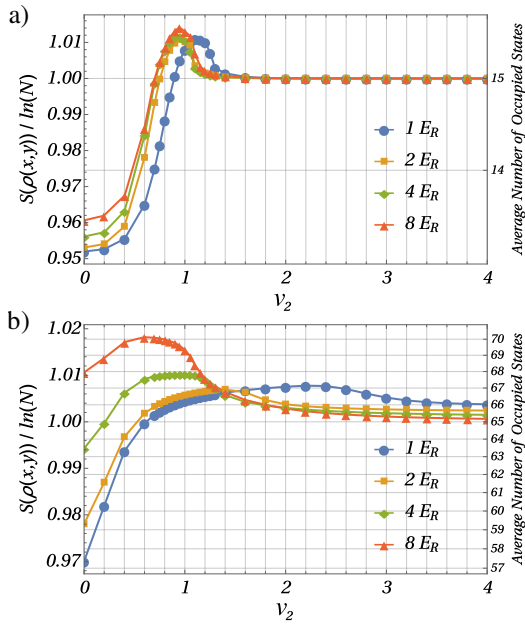


Figure 9. (Color online). Entropy of the RSPDM for (top) $N = 15$ and (bottom) $N = 65$ bosons in the Tonks-Girardeau regime.

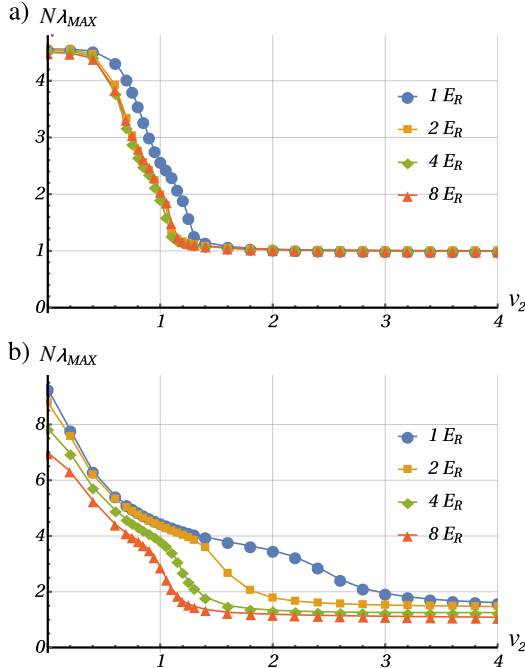


Figure 10. (Color online). Fraction of particles in the most largely occupied natural orbital, given by $N\lambda_{MAX}$ for a) $N_p = 15$ and b) $N_p = 65$ bosons in the Tonks-Girardeau regime.

in the momentum distribution of the system and in the entropy of the reduced single particle density matrix. Moreover in the case of bosons we have shown that the interaction plays a key role in the localization properties of the system.

VII. ACKNOWLEDGMENTS

NLG and FP acknowledge financial support from the EU collaborative project QuProcS (Grant Agreement 641277).

- [1] I. Bloch, J. Dalibard and W. Zwerger, Rev. Mod. Phys. **80**, 885 (2008).
- [2] M. Lewenstein, A. Sampera, V. Anufinger, B. Damski, A. Sen and U. Sen, Advances in Physics, **56**, 243 (2007).

- [3] Ph. Courteille, R.S. Freeland, D.J. Heinzen, F.A. van Abeelen and B.J. Verhaar, Phys. Rev. Lett. **81**, 69 (1998).
- [4] A. Polkovnikov et al., Rev. Mod. Phys. **83** 863 (2011)

- [5] I. Bloch, J. Dalibard and S. Nascimbene, *Nature. Phys.* **8** 267 (2012)
- [6] M. Modugno, *New J. Phys.* **11**, (2009).
- [7] S. Aubry and G. André, *Ann. Isr. Phys. Soc* **3**, 18 (1980).
- [8] P. G. Harper, *Proc. Phys. Soc. A* **68**, 874 (1955).
- [9] S. Y. Jitomirskaya, *Ann. of Math.* **150**, 1159 (1999).
- [10] E. B. Maciá, *Phys. Rev.* **B60**, 10032 (1999).
- [11] M. Girardeau, *J. Math. Phys.* **1**, 516 (1960).
- [12] M. Albert and P. Leboeuf, *Phys. Rev. A - At. Mol. Opt. Phys.* **81**, 1 (2010).
- [13] C. Aulbach, A. Wobst, G. L. Ingold, P. Hnggi, and I. Varga, *New J. Phys.* **6**, 1 (2004).
- [14] D. R. Grempel, S. Fishman, and R. E. Prange, *Phys. Rev. Lett.* **49**, 833 (1982).
- [15] G.-L. Ingold, A. Wobst, C. Aulbach, and P. Hnggi, *Eur. Phys. J. B* **30**, 7 (2002).
- [16] M. L. Sun, G. Wang, N. B. Li, and T. Nakayama, *EPL (Europhysics Lett.)* **110**, 57003 (2015).
- [17] G. Roux *et al*, *Phys. Rev.* **A78**, 023628 (2008);
- [18] T. Roscilde, *Phys. Rev.* **A77**, 063605 (2008)
- [19] X. Deng, *et al*, *Phys. Rev.* **A78**, 013625 (2008);
- [20] J. Biddle and S. Das Sarma, *Phys. Rev. Lett.* **104**, 1 (2010).
- [21] J. Biddle, D. J. Priour, B. Wang, and S. Das Sarma, *Phys. Rev. B - Condens. Matter Mater. Phys.* **83**, 1 (2011).
- [22] G. Wang, N. Li, and T. Nakayama, *2 Arxiv* 1312.0844 (2013).
- [23] D. J. Boers, B. Goedeke, D. Hinrichs, and M. Holthaus, *Phys. Rev. A - At. Mol. Opt. Phys.* **75**, 1 (2007).
- [24] R. Diener, G. Georgakis, J. Zhong, M. Raizen, and Q. Niu, *Phys. Rev. A* **64**, 33416 (2001).
- [25] S. Pilati, V. Kerala Varma, *arXiv:1610.06198* (2016)
- [26] R. Roth and K. Burnett, *Phys. Rev. A* **68**, 23604 (2003).
- [27] M. Larcher, F. Dalfovo, and M. Modugno, *Phys. Rev. A - At. Mol. Opt. Phys.* **80**, 1 (2009).
- [28] M. C. Gordillo, C. Carbonell-Coronado, and F. De Soto, *Phys. Rev. A - At. Mol. Opt. Phys.* **91**, 1 (2015).
- [29] M. D. Reichl and E. J. Mueller, *Phys. Rev. A - At. Mol. Opt. Phys.* **93**, 1 (2016).
- [30] H. Moritz, T. Stöferle, M. Köhl, and T. Esslinger, *Phys. Rev. Lett.* **91**, 250402 (2003).
- [31] M. Olshanii, *Phys. Rev. Lett.* **81**, 938 (1998).
- [32] M. Girardeau, *J. Math. Phys.* **1**, 516 (1960).
- [33] B. Damski, J. Zakrzewski, L. Santos, P. Zoller, and M. Lewenstein, *Phys. Rev. Lett.* **91**, 80403 (2003).
- [34] R. Roth and K. Burnett, *J. Opt. B Quantum Semiclassical Opt.* **5**, S50 (2003).
- [35] L. Fallani, J. E. Lye, V. Guarrera, C. Fort, and M. Inguscio, *Phys. Rev. Lett.* **98**, 1 (2007).
- [36] V. Guarrera, L. Fallani, J. E. Lye, C. Fort, and M. Inguscio, *New J. Phys.* **9**, 0 (2007).
- [37] L. Fallani, C. Fort, and M. Inguscio, *Adv. At. Mol. Opt. Phys.* **56**, 119 (2008).
- [38] G. Roati, C. D'Errico, L. Fallani, M. Fattori, C. Fort, M. Zaccanti, G. Modugno, M. Modugno, and M. Inguscio, *Nature* **453**, 895 (2008).
- [39] L. Tanzi, E. Lucioni, S. Chaudhuri, L. Gori, A. Kumar, C. D'Errico, M. Inguscio, and G. Modugno, *Phys. Rev. Lett.* **111**, 2 (2013).
- [40] M. Pillai, J. Goglio, and T. G. Walker, *Am. J. Phys.* **80**, 1017 (2012).
- [41] R. Pezer and H. Buljan, *Phys. Rev. Lett.* **98**, 240403 (2007).